Journal of MATERIALS RESEARCH

Invited Article
DOI: 10.1557/jmr.2018.478

UNDERSTANDING WATER-OXIDE INTERFACES TO HARNESS NEW PROCESSES AND TECHNOLOGIES

FOCUS ISSUE

Lateral water structure connects metal oxide nanoparticle faces

Piotr Zarzycki[1,a], Christopher A. Colla[1], Benjamin Gilbert[1], Kevin M. Rosso[2,b]

[1]Energy Geosciences Division, Lawrence Berkeley National Laboratory, Berkeley, California 94720, USA
[2]Physical Sciences Division, Pacific Northwest National Laboratory, Richland, Washington 99354, USA
[a)]Address all correspondence to this author. e-mail: ppzarzycki@lbl.gov
[b)]This author was an editor of this journal during the review and decision stage. For the *JMR* policy on review and publication of manuscripts authored by editors, please refer to http://www.mrs.org/editor-manuscripts/.

Received: 30 August 2018; accepted: 21 November 2018

When a metal oxide surface is immersed in aqueous solution, it has the ability to bind, orient, and order interfacial water, affecting both chemical and physical interactions with the surface. Structured interfacial water thus possesses time-averaged, spatially varying polarization charge and potential that are comparable to those arising due to ion accumulation. It is well established that interfacial water structure propagates from the surface into bulk solution. Here, we show that interfacial water structure also propagates laterally, with important consequences. The constant pH molecular dynamics was used to impose a pH difference between opposite faces of a model goethite (α-FeOOH) nanoparticle and quantify water polarization charge on intervening faces. We find that the structure of water on one face is strongly affected by the structure on nearby surfaces, revealing the importance of long-range lateral hydrogen bonding networks with implications for particle aggregation, oriented attachment, and processes such as dissolution and growth.

Introduction

Metal oxide minerals are an abundant and reactive component of the Earth's crust [1]. When oxides are immersed in aqueous solution, their surfaces acquire charge due to the ionization or dissociation of the surface oxo groups (i.e., protonation and deprotonation of surface exposed oxygen atoms) and preferential adsorption of ions [2, 3, 4, 5, 6]. In electrolyte solutions, the surface excess charge is compensated by the layers of ions of opposite charge to the surface (counter-ions) and of similar charge (co-ions) [2, 3, 4, 5, 6]. As a result, the equilibrium charge distribution at the interface, known as the electrical double layer (EDL), is established (Fig. 1) [2, 3, 4, 5, 6]. The EDL strongly influences the reactivity of all hydrated oxide mineral surfaces, with impacts in environmental systems such as controlling pollutant remediation and element cycles in soils and groundwater. EDL models of the metal oxide/electrolyte interface consist of surface protonation reactions (e.g., 1-pK [10] and 2-pK [11] models), the ion binding reactions, and the spatial distribution of counter-ions and co-ions charge. The thermodynamic descriptions of the EDL are based on models for the geometrical localization of the surface charge and electrolyte ions. The most detailed analytical descriptions of the EDL (e.g., the triple-layer model [11, 12]) divide the interface structure into layers that neglect lateral heterogeneity [2, 3, 4, 5, 6]. Moreover, water is modeled as a structureless, inert medium with a dielectric constant between 4 and 10 [3, 13]. The value of ε is most frequently approximated as 6 because it corresponds to the hypothetical situation of dielectrically saturated water in which all water dipoles are aligned with the electric field and act as though they are not associated (i.e., not hydrogen-bonded) [14]. This extreme regime corresponds to the dielectric constant of water at high frequency (ε_∞ = 5.2–6.0) [15].

Experimental studies [16, 17, 18, 19, 20, 21] and molecular simulations [22, 23, 24, 25, 26, 27, 28, 29] of the hydrated interface offer an entirely different view of the properties and roles of water in the EDL: interfacial water is highly structured and the structured water layers generate a polarization potential capable of screening effectively the surface potential. For instance, molecular dynamics (MD) simulations showed that the electrostatic potential at the AgCl/KCl electrolyte interface due to water orientation is larger than the potential arising due

https://doi.org/10.1557/jmr.2018.478 Published online by Cambridge University Press

© Materials Research Society 2019

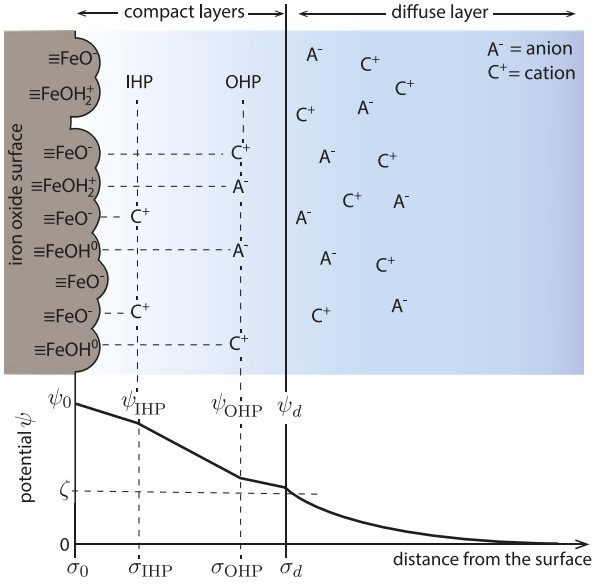


Figure 1: Illustration of the EDL model (four-layer model) of iron oxide/electrolyte interface [7, 8, 9]. The surface potential (ψ_0) is due to the protonation/deprotonation of the surface exposed FeOH groups; the electrokinetic potential (ζ) is formed at the shear plane of the EDL (i.e., near the boundary between the rigid and diffuse part of the EDL). The compact layer of the specifically adsorbed counter- and co-ions is referred to as inner Helmholtz plane (IHP) and the electrostatically bound counter- and co-ions as the outer Helmholtz plane (OHP). The diffuse part of the EDL is described by the Gouy–Chapman theory.

to the electrolyte ion distribution [28, 29]. This is in striking contrast to the analytical electrochemical calculations in which water structure is considered as structureless continuum that only changes the strength of the electrostatic interactions by lowering the dielectric constant at the surface (ε is supposed to be restored to its bulk value at distances >6 Å from the electrode surface) [14].

To date, there is lack of a complete understanding of the extent of interfacial water structure formation and the consequences for metal oxide surface processes that occur within the EDL. MD simulations predict that interfacial water layering causes significant energy barriers for ion adsorption and formation of outer- and inner-sphere complexes [e.g., Fe(II) at goethite, α-FeOOH] [29, 30]. However, the development of interfacial polarization potentials has not been included in any EDL models of the oxide/electrolyte interface. Recently, we developed a constant pH molecular dynamics (cpHMD) [31, 32] method incorporating surface charge constraints [30] that is capable of simulating oxide surface protonation/deprotonation processes, and associated solution dynamics, over timescales inaccessible to conventional MD. Here, we describe a simulation method designed to obtain further insight into the coupling between water ordering and a resulting polarization potential at vicinal surfaces exposed by a goethite nanoparticle (α-FeOOH). Our simulation results have important new implications for a wide range of chemical and physical processes controlled by the structure and dynamics at metal oxide/water interfaces, including particle aggregation and oriented attachment, precipitation–dissolution, mineral recrystallization, and coupled reactivity of confined hydrated surfaces.

Theory and implementation

There are numerous molecular simulation studies of charged metal oxide/electrolyte interfaces, but there are very few that implicitly considered the pH-dependent surface charge dynamics [33, 34, 35, 36, 37, 38, 39, 40]. Most of the reported molecular modeling studies were carried out using the charge neutral surfaces and therefore describe the surfaces at the pH corresponding to the point of zero charge (PZC). One of the first approaches to actually model proton release and binding to the metal oxide surfaces and to computationally validate the surface protonation models (e.g., 1-pK) was introduced by Borkovec et al. [33, 34]. Inspired by these papers, a similar stochastic simulation model was implemented, which also includes surface heterogeneity effects, electrolyte ion binding, and correlation [36, 37, 38, 39, 41, 42, 43, 44, 45]. These early simulation models, however, considered water only implicitly (as a dielectric continuum) and reduced the actual metal oxide surfaces to the lattice composed of the protonatable surface sites (i.e., as a discrete charge Ising model) [33, 34, 36, 37, 38, 39, 41, 42, 43, 44, 45]. The first fully-atomistic simulations of the charged metal oxide/electrolyte interface with pH-dependent surface charge and the explicit water models were carried out by Rustad et al. [35, 40]. Here, the simulation results obtained by using the cpHMD algorithm are presented. The cpHMD methodology has been developed originally for the biological systems [31], but recently, it was also adopted for the goethite/electrolyte interface [32].

The cpHMD algorithm alternates Monte Carlo (MC) sampling of the accessible protonation configurations and MD simulations of the response to altered charge distributions [31, 32]. As described, in more detail, elsewhere [30, 32], we use the replica-exchange approach to model dynamic proton redistribution. From a given protonation state *i*, our code generates a number of new protonation states (replicas) by swapping H^+ between surface hydroxyl groups with the constraint that the total surface charge of a given crystal face remains unchanged. This constraint allows the dynamic redistribution of H^+ ions on a given crystal face but does not allow them to move from one crystal face to another. The atomic configuration of each new protonation replica is subsequently optimized (using steepest descent energy minimization) and the solvent is allowed to reorganize for 100 ps using the MD simulation routine. Among all replicas, our simulation

https://doi.org/10.1557/jmr.2018.478 Published online by Cambridge University Press

© Materials Research Society 2019

algorithm selected the lowest energy one as a candidate for the new protonation state j, which is accepted either if it has a lower energy than the current H^+ proton redistribution i or if it satisfies the Metropolis–Hastings acceptance function:

$$P(i \to j) = \min\left(1, \exp\left(-\frac{\Delta U}{k_B T}\right)\right) \quad , \tag{1}$$

where $\Delta U = \Delta U^{vdw} + \Delta U^{elec}$ is the potential energy difference between j and i protonation states.

In the MC and MD steps, the long-range electrostatic energy was calculated using the classical Ewald summation scheme, in which the electrostatic energy U^{elec} is given by the following equation [46]:

$$4\pi\varepsilon_0 U^{elec} = \frac{2\pi}{V}\sum_{\vec{k}\neq 0}\frac{\left|S\left(\vec{k}\right)\right|^2}{k^2} e^{-\frac{k^2}{4\alpha}} + \frac{1}{2}\sum_{n\neq m}^{N}\frac{q_n q_m}{r_{nm}}\mathrm{erfc}\left(r_{nm}\sqrt{\alpha}\right) - \sqrt{\frac{\alpha}{\pi}}\sum_{n}^{N} q_n^2 \quad , \tag{2}$$

where n and m are run-over ion indexes, N is the total number of charged ions in the system, V is the cell volume, $\vec{k}$ is a vector in the reciprocal (Fourier) space, r_{nm} is the distance between the ions n and m, and erfc is the complementary error function (i.e., $\frac{2}{\sqrt{\pi}}\int_{r_{nm}\sqrt{\alpha}}^{\infty} e^{-x^2} dx$). The term $S\left(\vec{k}\right)$ is the charge structure factor and describes the Gaussian-smeared charge density in the reciprocal space [i.e., $\sum_{n}^{N} q_n \exp\left(i\vec{k}\cdot\vec{r}_n\right)$], i is the imaginary unit].

The electrostatic contribution to forces acting on an ion n is obtained by differentiation of U^{elect} with respect to r_n (i.e., $\vec{f}_n = -\frac{dU}{d\vec{r}_n}$):

$$-4\pi\varepsilon_0 \vec{f}_n^{elec} = \frac{q_n i\pi}{V}\sum_{\vec{k}\neq 0}\frac{\vec{k}\left(S\left(\vec{k}\right)\right)}{k^2} e^{i\vec{k}\cdot\vec{r}_n - \frac{k^2}{4\alpha}} - q_n\sum_{m\neq n}^{N}\frac{q_m}{r_{nm}}\left(\frac{\mathrm{erfc}(r_{nm}\sqrt{\alpha})}{r_{nm}} + 2\sqrt{\frac{\alpha}{\pi}} e^{-\alpha r_{nm}^2}\right)\frac{\vec{r}_{nm}}{r_{nm}} \quad , \tag{3}$$

which is derived using $\frac{d\mathrm{erfc}(r_n\sqrt{\alpha})}{dr_n} = -2e^{-\alpha r_n^2}\sqrt{\frac{\alpha}{\pi}}$ and $\frac{d\left|S\left(\vec{k}\right)\right|^2}{dr_n} = 2q_n i\vec{k} e^{i\vec{k}r_n} S\left(\vec{k}\right)$. The cutoff distance (10 Å) was applied for the short-range interactions and the real part of the Ewald sum. Equation (11) is used in calculating forces in MD part of the cpHMD algorithm. The time evolution of the system in the MD part is obtained by using the three-step velocity Verlet algorithm [47]:

$$\vec{r}_i(t+\delta t) = \vec{r}_i(t) + \vec{v}_i(t)\delta t + \frac{1}{2}(\delta t)^2\left(\vec{F}_i(t)/m_i\right) \quad , \tag{4}$$

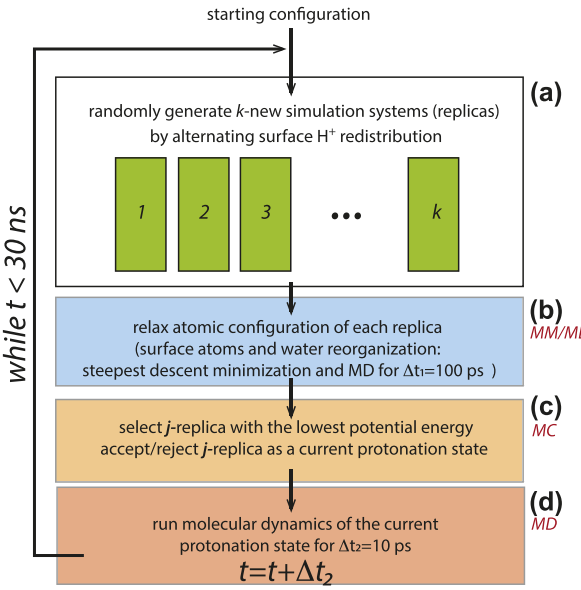


Figure 2: Diagram of the cpHMD algorithm: (a) generate a number of trial protonation states (replicas), (b) relax energy of each replica using MD, (c) the lowest energy relaxed protonation state is selected with weight given by Metropolis function for (d) the further system evolution.

$$\vec{v}_i\left(t+\frac{1}{2}\delta t\right) = \vec{v}_i(t) + \frac{1}{2}\delta t\left(\vec{F}_i(t)/m_i\right) \quad , \tag{5}$$

$$\vec{v}_i(t+\delta t) = \vec{v}_i\left(t+\frac{1}{2}\delta t\right) + \frac{1}{2}\delta t\left(\vec{F}_i(t+\delta t)/m_i\right) \quad , \tag{6}$$

where $\vec{r}_i$ and $\vec{v}_i$ are the i-atom position and velocity vectors, δt is the time step, and $\vec{F}_i/m_i$ is the acceleration of atom i. The rigid structure of the water molecule was preserved using the two-step RATTLE algorithm with the effective force $\vec{F}_i(t)$ in Eqs. (4)–(6) corrected by the bond-constraining force if atom i is bonded to any other atom [48].

MD simulations for a newly accepted protonation state were carried out for another 10 ps with a time step dt = 1 fs before attempting to change the protonation state by using the MC scheme [30]. A new protonation state used further in MD is the lowest energy replica among several generated from the current protonation state in parallel MC runs. The simulation algorithm is illustrated in Fig. 2.

The goethite nanoparticle used in this study and the force–field parameters are identical to those reported in our previous studies [30, 32], and inspired by related Fe(II)-catalyzed goethite re-crystallization experiments (Fig. 3) [49]. The particle exposes dominant {110} (in *Pbnm* space group) prismatic face terminations typical of needle-shaped crystallites. The charge-neutral particle is generated by protonating active surface oxygen sites in accordance with their expected proton affinities [50], with immersion in Simple Point Charge/Extended model (SPC/E) water and relaxation using

https://doi.org/10.1557/jmr.2018.478 Published online by Cambridge University Press

© Materials Research Society 2019

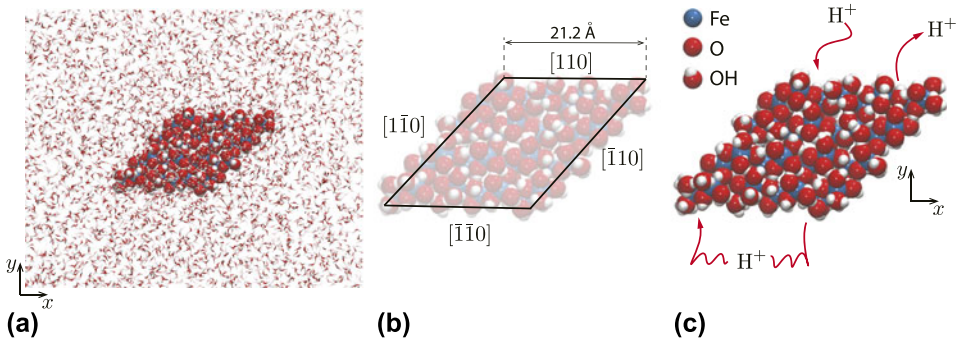


Figure 3: Illustrations of the simulation system. (a) The goethite (α-FeOOH) nanoparticle immersed in water. (b) Dimensions of the goethite nanoparticle. Each face is crystallographically equivalent. (c) H^+ ions populate surface sites at a density consistent with an assumed solution pH. Protons on each face redistribute according to the MC algorithm but are constrained to a single given face, enabling a pH difference to be imposed in some simulations.

the steepest descent algorithm. The subsequent temperature and density optimization steps were carried out using the NVT (canonical, constant number of particles N, volume V, and temperature T) and NPT (isothermal-isobaric, constant number of particles N, pressure P and temperature T) ensembles ($T = 298$ K, $P = 1$ atm., the Langevin thermostat with a collision frequency $\gamma = 2$ ps^{-1}, and the Berendsen thermostat–barostat) [30]. The cpHMD simulations were carried out for 30 ns and the configurations were saved every 0.1 ps. The parallelization was provided by the message passing interface [51, 52] library, and it allows to run the simulation in parallel using 4 nodes, each with 16 CPU cores (3.1 GHz Intel Xeon E52687W). The major performance bottlenecks were the Ewald summation procedure and writing simulation trajectory to the hard drive. A single cpHMD simulation run of 30 ns took around 9 days.

In order to simulate the interface structure at a given solution pH, protons are added or removed from surface sites to achieve a surface charge density consistent with experimentally determined titration curves [30].

Here, we study the effect of a surface charge imbalance between separated, crystallographically equivalent faces. Protons are transferred between opposite faces to achieve a protonation imbalance (ΔH^+) and then allowed to redistribute among sites on a single face but not to migrate between faces. Although this condition is not achievable in experimental systems, it provides a simple approach for studying lateral communication of water structure between mineral particle faces. Here, we report the simulation results of a goethite particle in the bulk water without any explicit electrolyte ions to isolate the effect of the water polarization potential. We will present the more complex simulation scenarios with a fully developed EDL of varying thickness in the future.

The most relevant analysis for this study is the calculation of surface electrostatic properties, which are defined via the Poisson's equation:

$$\nabla^2\psi = -\frac{\rho}{\varepsilon_0} = -\nabla \cdot E \quad , \tag{7}$$

where ψ is the electrostatic potential, ρ is the charge density, E is the electrostatic field, ε_0 is the static dielectric constant, and ∇ and ∇^2 are divergence and divergence of a gradient (Laplacian) operators, respectively.

The y-axis projections of the charge density, $\rho(y)$, and the electrostatic potential, $\psi(y)$, are obtained as follows [22, 23, 24, 25, 26, 27, 28, 29, 30]:

$$\rho(y) = \sum_{j=1}^{N} eq_j\delta(y_j - y), \quad \langle\rho(y)\rangle = \frac{1}{N_f}\sum_{i=1}^{N_f}\rho(y) \quad , \tag{8}$$

$$\psi(y) = -\frac{1}{\varepsilon_0}\int dy \int \langle\rho(y)\rangle dy \quad , \tag{9}$$

where δ is the Dirac delta function, e is the elementary charge, q_j is the charge on j-atom, ε_0 is the vacuum permittivity, and $\rho(y)$ is the time-averaged charge density profile (averaged over all trajectory frames, N_f). The two-dimensional charge density profile (projected on the x, y plane) is given by the following equation:

$$\langle\rho(x,y)\rangle = \frac{1}{N_f}\sum_{i=1}^{N_f}\sum_{j=1}^{N} eq_j\delta(y_j - y)\delta(x_j - x) \quad . \tag{10}$$

Finally, the net difference in the charge density between two simulation runs (i, j) that differ in the proton imbalance between the mirrored [110] and [$\bar{1}$10] faces, is given by the following equation:

$$\Delta\langle\rho(x,y)\rangle = \langle\rho(x,y)\rangle_i - \langle\rho(x,y)\rangle_j \quad . \tag{11}$$

The electrostatic properties and atomic densities calculated in this study are the time-averaged properties of the system that reflects the time-dependent evolution of all atoms and stochastic evolution of the protonation states.

Results

We first summarize the water ordering on a charge-neutral, proton-balanced goethite particle. The overall charge on the

https://doi.org/10.1557/jmr.2018.478 Published online by Cambridge University Press

© Materials Research Society 2019

nanoparticle is neutral, corresponding to a solution pH equals to the PZC ($pH_{PZC} \sim 9.1$) [30]. There is no potential difference imposed between equivalent faces, so $\Delta H^+ = 0$. In Fig. 4(a), the atomic densities and electrostatic potential are projected on the *y*-axis. The particle surface is defined by the peaks of surface protons [Figs. 4(a) and 4(b)]. The calculated electrostatic potential profile along the *y*-axis [Eq. (9)] shows near-surface modulation due to the layering of interfacial water [Figs. 4(b) and 4(c)]. The ordering decays with distance from the surface in an oscillating fashion, with a period corresponding to a typical water–water distance (3.1–3.2 Å). The predicted layering effect disappears at distances above ~15 Å for both the neutral [Figs. 4(b) and 4(c)] and charged surfaces. Water layer development has been observed in prior simulations [22, 23, 24, 25, 26, 27, 28, 29], but the present cpHMD simulation shows that the time-averaged structure develops even when surface protons are allowed redistribute dynamically as expected for natural interfaces.

In Fig. 5(a), the water charge density is averaged over the *z*-direction onto the *xy*-plane [Eq. (10)]. The charge maps were obtained from 30-ns simulation trajectories that were re-centered on the goethite particle. The negative charge (blue) corresponds to water oxygen atoms and the positive charge (red) corresponds to water hydrogen atoms. The semispherical shapes of the charge density spots in the first three water layers, as seen previously in conventional MD studies [53], are a manifestation of the limited rotational and translational mobilities of the interfacial water. Although the goethite surfaces have no net charge, they impart net polarization to the interfacial water. The charge density layers appear to be packed more densely at the particle edges than at the mid-surfaces. This is in good agreement with the predictions of a fully dissociable water model [40]. In each case, the edge atoms that are more water solvated exhibit higher proton affinity. As expected for the proton-balanced simulation, there are no differences in the polarization charge distribution on the equivalent faces.

To study the lateral propagation of water structure, we simulated a net charge-neutral but proton-imbalanced goethite nanoparticle, in which protons were transferred between two mirrored faces. Figure 5(b) displays the surface charge densities for a proton imbalance of $\Delta H^+ = 50$ applied to the top and bottom surfaces, corresponding to an equivalent solution pH of ~2.7 and ~13.4, respectively. The difference in the surface charge of our particle is much larger than expected in the actual system to more clearly observe the long-range correlation in the interfacial water polarization, but it represents the actual interactions between two adjacent surfaces. A visual comparison shows that the predicted structure of the polarized interface differs for $\Delta H^+ = 0$ [Fig. 5(a)] and $\Delta H^+ = 50$

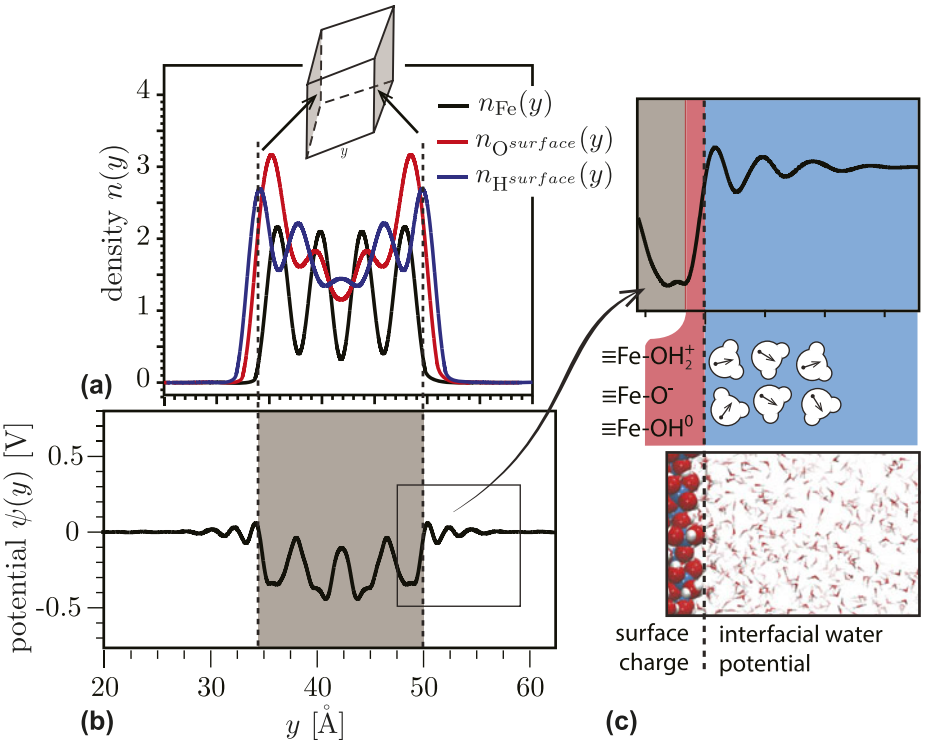


Figure 4: (a) Atomic density and (b, c) electrostatic potential profiles along the *y*-direction of particle with the charge-neutral surfaces. The water orientational response to the surface charge and interfacial layering results in the modulation of the electrostatic potential as a function of distance from the particle surface (b, c).

https://doi.org/10.1557/jmr.2018.478 Published online by Cambridge University Press

© Materials Research Society 2019

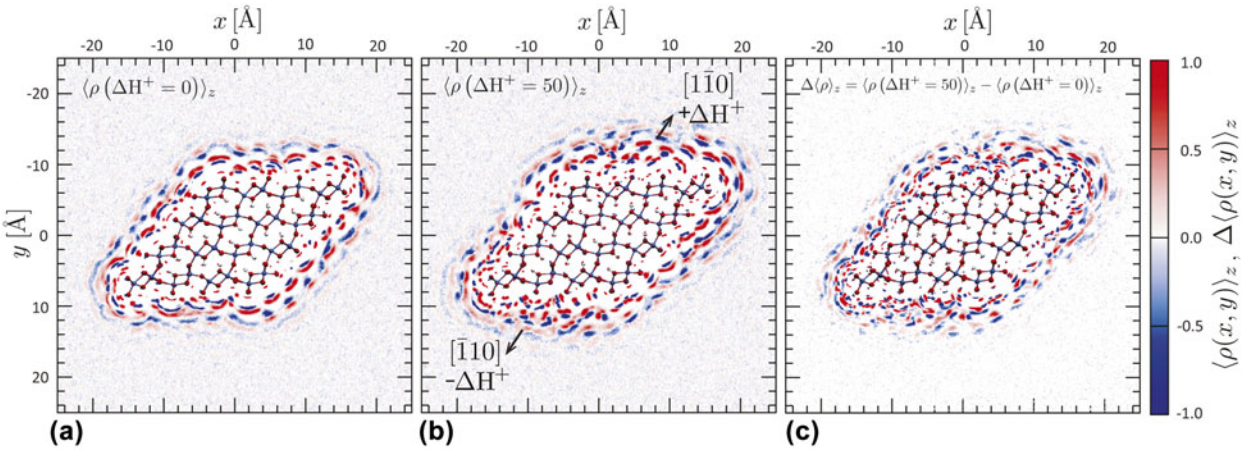


Figure 5: Maps of the time-averaged charge density of water molecules $\langle \rho(x, y)\rangle$ around a single goethite nanoparticle in water in μC/nm^3. (a) A charge-neutral, proton-balanced particle with all faces equivalent. (b) A charge-neutral, proton-imbalanced particle. The (110) face is positively charged ($\Delta H^+ = +50$), whereas the $(\bar{1}\bar{1}0)$ face is negatively charged ($\Delta H^+ = -50$). (c) Map of the difference in the time-averaged charge densities displayed in (a) and (b) (converted to e/nm^3 to preserve the color scale).

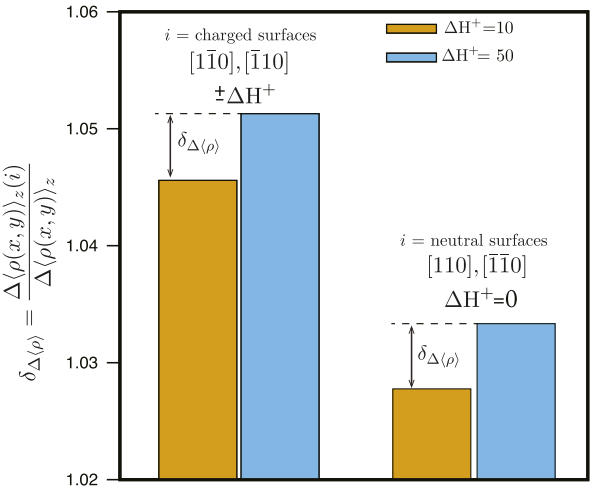


Figure 6: Histograms showing the relative differences in the integrated water polarization charge density between surface pairs. The left columns show the relative difference between charged surfaces for two values of the imposed charge: $\Delta H^+ = 50$ [Fig. 5(c)] and $\Delta H^+ = 10$ (an additional simulation not shown). The right columns show the relative differences in water polarization charge density between the pair of neutral surfaces.

[Fig. 5(b)]. For visual clarity, in Fig. 5(c), we plotted the charge density difference between the proton-balanced and the proton-imbalanced nanoparticles. If the water structure on each face is affected only by the net charge density, on that face we would expect that the difference maps for the bystander faces will be close to zero. Instead, the charge density difference maps reveal that water structure on all six faces is highly sensitive to protonation changes made at only two of the faces.

In Fig. 6, we provide simulation-averaged quantification of the effect by integrating the relative change in the net water polarization charge density [i.e., Fig. 5(c)] at the charged surfaces ($\Delta H^+ = 50$) and vicinal surfaces, where $\Delta H^+ = 0$. When two mirrored surfaces become charged, we observe a significant change in the water polarization on those surfaces compared with the case, in which the goethite nanoparticle has only net neutral surfaces (left columns in Fig. 6). We further observe that the unaltered surfaces also exhibit an increase in water polarization (right columns in Fig. 6). For all surfaces, the effect increases with increasing charge imbalance. The present study is limited to a single-geometry goethite nanoparticle with ~21 Å dimensions, and more work will be required to determine the distance over which water polarization can propagate laterally. Nevertheless, as discussed below, this phenomenon is relevant to a range of processes, such as particle-oriented aggregation, dissolution, precipitation, and interfacial reactivity.

Discussion

The present study is to our knowledge the first demonstration that the structure of interfacial water on an oxide mineral termination face is not independent of the water structure on neighboring faces. Rather, lateral hydrogen bond networks propagating from a highly charged face with polarized water molecules can strongly influence the order on neighboring faces. The actual particle will have a lower potential gradient and less pronounced polarization of interfacial water than shown in our simulations, but the same type of interactions between two adjacent surfaces will be present. This work demonstrates that the development of a polarized interface affects the time-averaged orientation of water at least three molecular distances away in both the perpendicular and lateral directions. This is an important finding, because it shows that the water structuring at the interface is due to a competition between the water propensity to preserve a tetrahedral

https://doi.org/10.1557/jmr.2018.478 Published online by Cambridge University Press

© Materials Research Society 2019

hydrogen bond network and to align with the electric field generated by the charged surface. This prediction is consistent with recent experimental and simulation studies that have provided an increasingly detailed three-dimensional depiction of the molecular structure of EDLs in aqueous systems and macromolecular systems, including ionic liquids [57, 58, 59, 60].

It remains a challenge to incorporate nanoscale and molecular scale phenomena into computationally tractable analytical models of EDL properties. Recent contributions have described modified EDL models incorporating interface roughness [41, 42, 43, 44, 45, 61] or finite ion correlations [42, 62, 63, 64, 65, 66]. In principle, classical EDL models could incorporate both vertical and lateral water polarization phenomena if the Poisson's equation [Eq. (7)] is solved in all three dimensions, that is:

$$\nabla\varepsilon(x,y,z)\nabla\psi(x,y,z) = -\frac{\rho(x,y,z)}{\varepsilon_0}\Delta\langle\rho(x,y)\rangle \quad , \qquad (12)$$

where the lateral and vertical water ordering and polarization are included via the spatially dependent dielectric constant $\varepsilon(x, y, z)$. Similar to the 1D case, the pH-dependent surface charge of metal oxides with acidic surface sites will provide a boundary condition. In order to develop and test new EDL models that incorporate lateral water polarization, it will be essential to further apply the cpHMD approach described here. Planned future work includes elucidating the general functional form of $\varepsilon(x, y, z)$, its relationship with the nature and charge state of the oxide surface [i.e., boundary conditions to Eq. (12)], and the influence of counter- and co-ions.

Although the present simulation concerns a single nanoparticle, the consequences are broad because they show that the reactivity of all faces exposed by a particle is coupled through the hydrogen bond network. For example, in an important non-classical pathway for mineral growth—oriented attachment of nanoparticles—interfacial water ordering appears to play an important guiding role in the establishment of matching crystal lattice orientations between mineral grains required for fusion [54]. Indeed, Zhang et al. [55, 56] showed that the self-organization of intervening water between two approaching zinc oxide particles is critical for establishing a rotational force between misoriented surfaces. Our work demonstrates that interfacial water is connected across all exposed particle surfaces. Hence, the vicinal surfaces can influence the orientation forces between two opposite faces, and through lateral reorganization of water on adjacent surfaces, successful attachment events could alter the propensity for subsequent attachment events.

There is also increasing evidence that interfacial redox processes at iron oxide surfaces are influenced by long-range coupling between electron and proton transfer. Yanina et al. [67] demonstrated the action of internal electron conduction between crystallographically distinct faces of hematite undergoing redox reaction. Internal conduction is likely an important mechanism enabling atom exchange in systems of goethite and aqueous Fe(II), as identified by isotope tracer studies [49]. Interfacial processes that can contribute to electrical conduction include fluctuations in protonation/deportation, which create transient field gradients that can couple to charge transfer [32]. Fast conduction channels that run parallel to the interfacial plane [29] would therefore be susceptible the structure and repolarization dynamics of interfacial water molecules. The present work indicates that the propagation of water structure between faces will alter the surface polarization responsible for establishing internal electric fields.

Conclusions

The orientation of water in the first few layers at a given metal oxide nanoparticle surface is sensitive to the surface charge state of neighboring surfaces. The phenomenon is caused by the lateral propagation of ordered water structure, a new type of long-range electrostatic communication between oxide surfaces. Such lateral water ordering implies the need for more sophisticated models for EDL structure, with anisotropic dynamics in three dimensions, incorporating lateral polarization structure within single faces and between faces. Although our simulation study employs a particle with the exaggerated charge difference between faces, the lateral communication through the interfacial water polarization exists in any mineral particle suspension. Many important metal oxide–water chemical and physical processes, including ion-by-ion growth, oriented aggregation, and interfacial charge transfer reactions, are likely to be influenced by these long-range interactions.

Acknowledgments

This material is based on work supported by the U.S. Department of Energy, Office of Science, Office of Basic Energy Sciences, Chemical Sciences, Geosciences, and Biosciences Division, through its Geosciences programs at LBNL (under Contract DE-AC02-05CH11231) and PNNL.

References

1. **W.M. White**: *Geochemistry* (Wiley, Chichester, West Sussex, UK, 2013).
2. **J. Lyklema**: *Fundamentals of Interface and Colloid Science: Solid-Liquid Iterfaces* (Elsevier, San Diego, 1995).
3. **W. Stumm and J.J. Morgan**: *Aquatic Chemistry: Chemical Equilibria and Rates in Natural Waters* (Wiley, New York, 1996).
4. **G.E. Brown, V.E. Henrich, W.H. Casey, D.L. Clark, C. Eggleston, A. Felmy, D.W. Goodman, M. Grätzel, G. Maciel, M.I. McCarthy, K.H. Nealson, D.A. Sverjensky, M.F. Toney, and**

https://doi.org/10.1557/jmr.2018.478 Published online by Cambridge University Press

© Materials Research Society 2019

J.M. Zachara: Metal oxide surfaces and their interactions with aqueous solutions and microbial organisms. *Chem. Rev.* **99**, 77 (1999).

5. **G.E. Brown**: How minerals react with water. *Science* **294**, 67 (2001).
6. **G.E. Brown and G. Calas**: Mineral-aqueous solution interfaces and their impact on the environment. *Geochem. Perspect.* **1**, 483 (2012).
7. **L. Bousse and J.D. Meindl**: *Geochemical Processes at Mineral Surfaces* (American Chemical Society, Washington, DC, 1987); pp. 79–98.
8. **J.W. Bowden, S. Nagarajah, N.J. Barrow, A.M. Posner, and J.P. Quirk**: Describing the adsorption of phosphate, citrate and selenite on a variable-charge mineral surface. *Soil Res.* **18**, 49 (1980).
9. **R. Charmas, W. Piasecki, and W. Rudzinski**: Four layer complexation model for ion adsorption at electrolyte/oxide interface: Theoretical foundations. *Langmuir* **11**, 3199 (1995).
10. **W.H. van Riemsdijk, J.C.M. de Wit, L.K. Koopal, and G.H. Bolt**: Metal ion adsorption on heterogeneous surfaces: Adsorption models. *J. Colloid Interface Sci.* **116**, 511 (1987).
11. **J.A. Davis, R.O. James, and J.O. Leckie**: Surface ionization and complexation at the oxide/water interface: I. Computation of electrical double layer properties in simple electrolytes. *J. Colloid Interface Sci.* **63**, 480 (1978).
12. **D.E. Yates, S. Levine, and T.W. Healy**: Site-binding model of the electrical double layer at the oxide/water interface. *J. Chem. Soc., Faraday Trans. 1* **70**, 1807 (1974).
13. **O. Björneholm, M.H. Hansen, A. Hodgson, L-M. Liu, D.T. Limmer, A. Michaelides, P. Pedevilla, J. Rossmeisl, H. Shen, G. Tocci, E. Tyrode, M-M. Walz, J. Werner, and H. Bluhm**: Water at interfaces. *Chem. Rev.* **116**, 7698 (2016).
14. **J.O. Bockris and S.U.M. Khan**: *Surface Electrochemistry: A Molecular Level Approach* (Springer, New York, 1993).
15. **V. Raicu and Y. Feldman**: *Dielectric Relaxation in Biological Systems: Physical Principles, Methods, and Applications* (Oxford University Press, Oxford, UK, 2015).
16. **M.F. Toney, J.N. Howard, J. Richer, G.L. Borges, J.G. Gordon, O.R. Melroy, D.G. Wiesler, D. Yee, and L.B. Sorensen**: Voltage-dependent ordering of water molecules at an electrode–electrolyte interface. *Nature* **368**, 444 (1994).
17. **Y.R. Shen and V. Ostroverkhov**: Sum-frequency vibrational spectroscopy on water interfaces: Polar orientation of water molecules at interfaces. *Chem. Rev.* **106**, 1140 (2006).
18. **M.A. Henderson**: The interaction of water with solid surfaces: Fundamental aspects revisited. *Surf. Sci. Rep.* **46**, 1 (2002).
19. **J. Carrasco, A. Hodgson, and A. Michaelides**: A molecular perspective of water at metal interfaces. *Nat. Mater.* **11**, 667 (2012).
20. **P. Fenter and N.C. Sturchio**: Mineral–water interfacial structures revealed by synchrotron X-ray scattering. *Prog. Surf. Sci.* **77**, 171 (2004).
21. **J.N. Israelachvili and R.M. Pashley**: Molecular layering of water at surfaces and origin of repulsive hydration forces. *Nature* **306**, 249 (1983).
22. **E. Spohr**: Molecular simulation of the electrochemical double layer. *Electrochim. Acta* **44**, 1697 (1999).
23. **A. Wieckowski**: *Interfacial Electrochemistry: Theory: Experiment, and Applications* (CRC Press, New York, 1999).
24. **J. Wang, A.G. Kalinichev, and R.J. Kirkpatrick**: Effects of substrate structure and composition on the structure, dynamics, and energetics of water at mineral surfaces: A molecular dynamics modeling study. *Geochim. Cosmochim. Acta* **70**, 562 (2006).
25. **S.H. Lee and P.J. Rossky**: A comparison of the structure and dynamics of liquid water at hydrophobic and hydrophilic surfaces—A molecular dynamics simulation study. *J. Chem. Phys.* **100**, 3334 (1994).
26. **M.R. Philpott and J.N. Glosli**: Electric potential near a charged metal surface in contact with aqueous electrolyte. *J. Electroanal. Chem.* **409**, 65 (1996).
27. **P. Zarzycki, S. Kerisit, and K.M. Rosso**: Molecular dynamics study of the electrical double layer at silver chloride- electrolyte interfaces. *J. Phys. Chem. C* **114**, 8905 (2010).
28. **P. Zarzycki and K.M. Rosso**: Molecular dynamics simulation of the AgCl/electrolyte interfacial capacity. *J. Phys. Chem. C* **114**, 10019 (2010).
29. **P. Zarzycki, S. Kerisit, and K.M. Rosso**: Molecular dynamics study of Fe(II) adsorption, electron exchange, and mobility at goethite (α-FeOOH) surfaces. *J. Phys. Chem. C* **119**, 3111 (2015).
30. **P. Zarzycki and K.M. Rosso**: Surface charge effects on Fe(II) sorption and oxidation at (110) goethite surfaces. *J. Phys. Chem. C* **122**, 10059 (2018).
31. **J. Mongan, D.A. Case, and J.A. McCammon**: Constant pH molecular dynamics in generalized born implicit solvent. *J. Comput. Chem.* **25**, 2038 (2004).
32. **P. Zarzycki, D.M. Smith, and K.M. Rosso**: Proton dynamics on goethite nanoparticles and coupling to electron transport. *J. Chem. Theory Comput.* **11**, 1715 (2015).
33. **M. Borkovec**: Origin of 1-pK and 2-pK models for ionizable water–solid interfaces. *Langmuir* **13**, 2608 (1997).
34. **M. Borkovec, J. Daicic, and G.J.M. Koper**: Ionization properties of interfaces and linear polyelectrolytes: A discrete charge Ising model. *Phys. A* **298**, 1 (2001).
35. **J.R. Rustad, E. Wasserman, A.R. Felmy, and C. Wilke**: Molecular dynamics study of proton binding to silica surfaces. *J. Colloid Interface Sci.* **198**, 119 (1998).
36. **P. Zarzycki**: Computational study of proton binding at the rutile/electrolyte solution interface. *J. Phys. Chem. C* **111**, 7692 (2007).
37. **P. Zarzycki**: Comparison of the Monte Carlo estimation of surface electrostatic potential at the hematite (0001)/electrolyte interface with the experiment. *Appl. Surf. Sci.* **253**, 7604 (2007).
38. **P. Zarzycki and K.M. Rosso**: Nonlinear response of the surface electrostatic potential formed at metal oxide/electrolyte interfaces. A Monte Carlo simulation study. *J. Colloid Interface Sci.* **341**, 143 (2010).

https://doi.org/10.1557/jmr.2018.478 Published online by Cambridge University Press

© Materials Research Society 2019

39. **P. Zarzycki, S. Chatman, T. Preočanin, and K.M. Rosso**: Electrostatic potential of specific mineral faces. *Langmuir* **27**, 7986 (2011).
40. **J.R. Rustad and A.R. Felmy**: The influence of edge sites on the development of surface charge on goethite nanoparticles: A molecular dynamics investigation. *Geochim. Cosmochim. Acta* **69**, 1405 (2005).
41. **P. Zarzycki**: Monte Carlo simulation of the electrical differential capacitance of a double electrical layer formed at the heterogeneous metal oxide/electrolyte interface. *J. Colloid Interface Sci.* **297**, 204 (2006).
42. **P. Zarzycki**: Monte Carlo modeling of ion adsorption at the energetically heterogeneous metal oxide/electrolyte interface: Micro- and macroscopic correlations between adsorption energies. *J. Colloid Interface Sci.* **306**, 328 (2007).
43. **P. Zarzycki**: Monte Carlo study of the topographic effects on the proton binding at the energetically heterogeneous metal oxide/electrolyte interface. *Langmuir* **22**, 11234 (2006).
44. **P. Zarzycki, R. Charmas, and P. Szabelski**: Study of proton adsorption at heterogeneous oxide/electrolyte interface. Prediction of the surface potential using Monte Carlo simulations and 1-pK approach. *J. Comput. Chem.* **25**, 704 (2004).
45. **P. Szabelski, P. Zarzycki, and R. Charmas**: A Monte Carlo study of proton adsorption at the heterogeneous oxide/electrolyte interface. *Langmuir* **20**, 997 (2004).
46. **D. Frenkel and B. Smit**: *Understanding Molecular Simulations: From Algorithms to Applications* (Academic Press, San Diego, 2002).
47. **W.C. Swope, H.C. Andersen, P.H. Berens, and K.R. Wilson**: A computer simulation method for the calculation of equilibrium constants for the formation of physical clusters of molecules: Application to small water clusters. *J. Chem. Phys.* **76**, 637 (1982).
48. **H.C. Andersen**: Rattle: A "velocity" version of the shake algorithm for molecular dynamics calculations. *J. Comput. Phys.* **52**, 24 (1983).
49. **R.M. Handler, A.J. Frierdich, C.M. Johnson, K.M. Rosso, B.L. Beard, C. Wang, D.E. Latta, A. Neumann, T. Pasakarnis, W.A.P.J. Premaratne, and M.M. Scherer**: Fe(II)-catalyzed recrystallization of goethite revisited. *Environ. Sci. Technol.* **48**, 11302 (2014).
50. **P. Venema, T. Hiemstra, P.G. Weidler, and W.H. van Riemsdijk**: Intrinsic proton affinity of reactive surface groups of metal (Hydr) oxides: Application to iron (Hydr)oxides. *J. Colloid Interface Sci.* **198**, 282 (1998).
51. **D.W. Walker and J.J. Dongarra**: MPI: A standard message passing interface. *Supercomputer* **12**, 56 (1996).
52. **W. Gropp, E. Lusk, N. Doss, and A. Skjellum**: A high-performance, portable implementation of the MPI message passing interface standard. *Parallel Comput.* **22**, 789 (1996).
53. **D. Spagnoli, B. Gilbert, G.A. Waychunas, and J.F. Banfield**: Prediction of the effects of size and morphology on the structure of water around hematite nanoparticles. *Geochim. Cosmochim. Acta* **73**, 4023 (2009).
54. **J.J. De Yoreo, U.P. Pupa, A.J. Nico, R. Lee Penn, S. Whitelam, D. Joester, H. Zhang, J.D. Rimer, A. Navrotsky, J.F. Banfield, A.F. Wallace, F. Marc Michel, F.C. Meldrum, H. Cölfen, and P.M. Dove**: Crystallization by particle attachment in synthetic, biogenic, and geologic environments. *Science* **349**, aaa6760 (2015).
55. **X. Zhang, Y. He, M.L. Sushko, J. Liu, L. Luo, J.J. De Yoreo, S.X. Mao, C. Wang, and K.M. Rosso**: Direction-specific van der Waals attraction between rutile TiO_2 nanocrystals. *Science* **356**, 434 (2017).
56. **X. Zhang, Z. Shen, J. Liu, S.N. Kerisit, M.E. Bowden, M. L. Sushko, J.J. De Yoreo, and K.M. Rosso**: Direction-specific interaction forces underlying zinc oxide crystal growth by oriented attachment. *Nat. Commun.* **8**, 835 (2017).
57. **Y. Liu, Y. Zhang, G. Wu, and J. Hu**: Coexistence of liquid and solid phases of Bmim-PF_6 ionic liquid on mica surfaces at room temperature. *J. Am. Chem. Soc.* **128**, 7456 (2006).
58. **L. Tamam, B.M. Ocko, H. Reichert, and M. Deutsch**: Checkerboard self-patterning of an ionic liquid film on mercury. *Phys. Rev. Lett.* **106**, 197801 (2011).
59. **C. Merlet, D.T. Limmer, M. Salanne, R. van Roij, P.A. Madden, D. Chandler, and B. Rotenberg**: The electric double layer has a life of its own. *J. Phys. Chem. C* **118**, 18291 (2014).
60. **A.A. Kornyshev and R. Qiao**: Three-dimensional double layers. *J. Phys. Chem. C* **118**, 18285 (2014).
61. **M. Valtiner, X. Banquy, K. Kristiansen, G.W. Greene, and J.N. Israelachvili**: The electrochemical surface forces apparatus: The effect of surface roughness, electrostatic surface potentials, and anodic oxide growth on interaction forces, and friction between dissimilar surfaces in aqueous solutions. *Langmuir* **28**, 13080 (2012).
62. **A. Voukadinova, M. Valiskó, and D. Gillespie**: Assessing the accuracy of three classical density functional theories of the electrical double layer. *Phys. Rev. E* **98**, 012116 (2018).
63. **F. Jiménez-Ángeles and M. Lozada-Cassou**: A model macroion solution next to a charged wall: Overcharging, charge reversal, and charge inversion by macroions. *J. Phys. Chem. B* **108**, 7286 (2004).
64. **J. Forsman**: A simple correlation-corrected Poisson−Boltzmann theory. *J. Phys. Chem. B* **108**, 9236 (2004).
65. **M.L. Sushko and K.M. Rosso**: The origin of facet selectivity and alignment in anatase TiO_2 nanoparticles in electrolyte solutions: Implications for oriented attachment in metal oxides. *Nanoscale* **8**, 19714 (2016).
66. **Z. Shen, J. Chun, K.M. Rosso, and C.J. Mundy**: Surface chemistry affects the efficacy of the hydration force between two ZnO$(10\bar{1}\bar{0})$ surfaces. *J. Phys. Chem. C* **122**, 12259 (2018).
67. **S.V. Yanina and K.M. Rosso**: Linked reactivity at mineral-water interfaces through bulk crystal conduction. *Science* **320**, 218 (2008).

https://doi.org/10.1557/jmr.2018.478 Published online by Cambridge University Press

© Materials Research Society 2019